Dispersion and fidelity in quantum interferometry

D. S. Simon,[1] A. V. Sergienko,[1,2] and T. B. Bahder[3]
[1]*Department of Electrical and Computer Engineering, Boston University, 8 St. Mary's Street, Boston, Massachusetts 02215, USA*
[2]*Department of Physics, Boston University, 590 Commonwealth Avenue, Boston, Massachusetts 02215, USA*
[3]*Charles M. Bowden Research Facility, Aviation and Missile Research, Development, and Engineering Center, U.S. Army RDECOM, Redstone Arsenal, Alabama 35898, USA*
(Received 29 July 2008; published 26 November 2008)

We consider Mach-Zehnder and Hong-Ou-Mandel interferometers with nonclassical states of light as input, and study the effect that dispersion inside the interferometer has on the sensitivity of phase measurements. We study in detail a number of different one- and two-photon input states, including Fock, dual Fock, maximally path-entangled $|N,0\rangle+\langle 0,N|$ ("N00N") states, and photon pairs from parametric down-conversion. Assuming there is a phase shift ϕ_0 in one arm of the interferometer, we compute the probabilities of measurement outcomes as a function of ϕ_0, and then compute the Shannon mutual information between ϕ_0 and the measurements. This provides a means of quantitatively comparing the utility of various input states for determining the phase in the presence of dispersion. In addition, we consider a simplified model of parametric down-conversion for which probabilities can be explicitly computed analytically, and which serves as a limiting case of the more realistic down-conversion model.

DOI: 10.1103/PhysRevA.78.053829 PACS number(s): 42.50.St, 42.50.Dv, 07.60.Ly, 03.67.−a

I. INTRODUCTION

Interferometry is both an important tool for practical measurements and a useful testing ground for fundamental physical principles. As a result, the search for methods to improve the resolution of interferometers forms an active area of study. It has been shown by a number of authors ([1–4]) that nonclassical states, in particular those with high degrees of entanglement, when used as input to an interferometer can lead to resolutions that approach the Heisenberg limit, the fundamental physical limit imposed by the uncertainty principle. Most of this previous work has dealt with idealized interferometers, with no dispersion or photon losses. Before quantum interferometry may become a useful practical tool the question must be asked as to how well the conclusions of these previous studies hold up in more realistic and less idealized situations. In this paper, we will attempt to take the next step along this road by adding dispersion to the apparatus and examining what effect this has on the phase sensitivity of interferometry with nonclassical input. The motivation for this work is the desire to ultimately construct quantum sensors that can measure the values of external fields by measuring the phases shifts they produce in an interferometer.

In particular, the nonclassical input states we will consider are (i) Fock states $|N,0\rangle$ which have a fixed number of photons incident on one input port, (ii) dual or twin Fock states $|N,N\rangle$ which have the same number of photons incident on each input port, and (iii) $(1/\sqrt{2})$ $[|N,0\rangle+|0,N\rangle]$ (N00N states). Here, $|N_a,N_b\rangle$ denotes a state with numbers N_a and N_b of photons entering each of the two interferometer input ports.

There has been a great deal of recent work on the production of nonclassical states of light with large ($N>2$) numbers of photons by means of postselection (for example, [5–8]); however, at present the utility of these postselection schemes for application to practical situations is not clear. Although this work is useful for clarifying the scientific issues involved, it is not technologically feasible at present to use these methods to produce the desired states on demand. Rather, postselection produces states statistically, at random times, and therefore cannot be relied upon to produce states on demand for a quantum sensor. In addition, for large photon number, great care must be taken to distinguish between states of N photons and those of $N-1$ photons, making it difficult to prevent mixed states from appearing, which would change the physics involved. In contrast, two-photon entangled states with well-defined properties can be easily produced by parametric down-conversion or other methods.

Due to the current practical difficulties of producing on demand entangled photon states with large, well-defined N, we save the large-N case for later study and restrict ourselves in this current paper to situations which are both simpler and of more immediate practical interest, namely the cases of one or two photons. Furthermore, for the two-photon case, we consider two possibilities: (i) the photons may be uncorrelated in frequency, or (ii) the pair may be produced through spontaneous parametric down-conversion (SPDC), resulting in anticorrelation between the two frequencies.

Our goal is to compare the usefulness of each of these cases for making phase measurements in the presence of dispersion, so we will need a means of quantifying the sensitivity of the interferometer with respect to these measurements. Consider a single shot consisting of a nonclassical state of light with a fixed number of photons being injected into the input ports of the interferometer. Suppose some phase-dependent observable $M(\phi)$ is measured during this shot. The usual way to define the phase sensitivity of the measurement is by computing

$$\Delta\phi = \left|\frac{dM}{d\phi}\right|^{-1} \Delta M. \tag{1}$$

However, this is correct only if the probability distribution of the phases has a single peak and is approximately Gaussian

 ©2008 The American Physical Society

in shape. A more general strategy is to take an information-theoretical approach and to define the quantum fidelity by means of the Shannon mutual information [9]

$$H(\Phi{:}M) = \frac{1}{2\pi}\sum_m \int_{-\pi}^{\pi} d\phi\, P(m|\phi)\log_2\left(\frac{2\pi P(m|\phi)}{\int_{-\pi}^{\pi} P(m|\phi')d\phi'}\right). \tag{2}$$

Here, m and ϕ are the measured values of the random variables M and Φ, while $P(m|\phi)$ is the conditional probability of obtaining measurement m given the phase ϕ on a particular shot. In this formula, we have also assumed maximum ignorance of the phase, i.e., we have assumed a uniform distribution for ϕ, $p(\phi)=1/2\pi$. Suppose that the detectors have a characteristic time scale T_D. Then in this context, a single shot will consist of a well-defined number of photons entering the apparatus simultaneously (i.e., within a temporal window much smaller than T_D) and separated in time from any other entering photons by a time $\geqslant T_D$. The mutual information is a measure of the information gained per shot about the phase Φ from a measurement of the observable M. In our case, the role of M will be played by the number of photons detected at each of the output ports. For N input photons, output detector C will count l photons, detector D will detect the remaining $N-l$ photons, and the sum in Eq. (2) will become a sum over l, where $l=0,1,\ldots,N$. Throughout this paper we will use the quantum fidelity as our measure of phase sensitivity. Besides being of very general applicability and giving a precise, calculable measure for the utility of a measurement, the introduction of the mutual information provides a link to the theory of quantum information processing. Bahder and Lopata [9] have computed the quantum fidelity as a function of N for idealized lossless and dispersionless interferometers with Fock and N00N state inputs. In the following sections, we will see how their results change for the cases of $N=1$ and 2 when dispersion is present.

Although not the principal focus of this paper, it should be noted that the existence of multiple peaks in the output probability distributions invalidate the assumptions used to derive the Heisenberg bound from the Cramer-Rao lower bound, which makes input states with multimodal distributions especially interesting from the point of view of the study of phase sensitivity. Note that violations of the Heisenberg limit have recently been shown to exist in another context, distinct from the situation examined in this paper, namely, in the context of nonlinear interferometry [10–12].

We will assume that one branch of the interferometer has a dispersive element which gives the photon wave number k a frequency dependence of the form

$$k(\omega) = k_0 + \alpha(\omega-\omega_0) + \beta(\omega-\omega_0)^2, \tag{3}$$

ignoring the possibility of higher-order terms. The other interferometer arm will be assumed to be of negligible dispersion. Here, α is the inverse of the group velocity, and β is the group delay dispersion per unit length.

In addition to the Mach-Zehnder interferometer, we will examine the fidelity of an alternate setup used in [6], in which N00N states are incident on a single beam splitter used as a Hong-Ou-Mandel (HOM) interferometer. We will then be in a position to compare the possible input states and interferometer setups, with a view to gaining insight into their relative usefulness in practical measurements. In the two-photon cases, we must distinguish between situations in which the photon energies (or frequencies) are correlated and those in which they are independent. Thus, after we examine the case of energy-uncorrelated photons, we look at photon pairs anticorrelated in energy. We further consider two subcases of the latter: (i) a simple model which can be solved analytically and which amounts to a simplified version of spontaneous down-conversion, and (ii) a more realistic but less analytically tractable version of down-conversion.

The plan of this paper is as follows. In Sec. II we consider the setup for the dispersive Mach-Zehnder interferometer and define the input states we will use in more detail. In Sec. III, we apply the possible one-photon inputs to the interferometer and compute the probabilities for the various possible outcomes. In Secs. IV and V, respectively, we do the same for the Mach-Zehnder interferometer with several different two-photon inputs and for the HOM interferometer with $N=2$ N00N state input. In Sec. VI we compute and plot the mutual information for each of the preceding cases as functions of bandwidth and dispersion levels; we then compare and discuss the results for the various cases. Finally, in Sec. VII we repeat the same calculation for input consisting of a photon pair produced via spontaneous parametric down-conversion before arriving at final conclusions in Sec. VIII.

For ease of reference later, Table I summarizes the specific cases we will examine over the following sections.

II. THE DISPERSIVE MACH-ZEHNDER INTERFEROMETER

Consider the Mach-Zehnder interferometer of Fig. 1, with 50:50 beam splitters. Assume for the moment that there is no dispersion in the apparatus. Let $\hat{a}_\omega$ and $\hat{b}_\omega$ be operators that annihilate photon states in the two input ports A and B. They obey the usual canonical commutation relations with the corresponding creation operators $\hat{a}^\dagger_\omega$ and $\hat{b}^\dagger_\omega$:

$$[\hat{a}_\omega,\hat{a}^\dagger_{\omega'}] = [\hat{b}_\omega,\hat{b}^\dagger_{\omega'}] = \delta(\omega-\omega'), \tag{4}$$

with all other commutators vanishing. For independent photons, the input states to the interferometer can be described in terms of the number of photons entering the two ports:

$$|N_a,N_b;\omega_1,\ldots,\omega_{N_a};\omega'_1,\ldots,\omega'_{N_b}\rangle = \frac{1}{\sqrt{N_a!N_b!}}\hat{a}^\dagger_{\omega_1}\cdots\hat{a}^\dagger_{\omega_{N_a}}\hat{b}^\dagger_{\omega'_1}\cdots\hat{b}^\dagger_{\omega'_{N_b}}|0\rangle, \tag{5}$$

where N_a and N_b are the number of photons in ports A and B, respectively, and $|0\rangle$ is the vacuum state with no photons. Similarly, N_c, N_d, $\hat{c}_\omega$, and $\hat{d}_\omega$ will represent the photon numbers and annihilation operators at output ports C and D.

The effect of the Mach-Zehnder (MZ) interferometer on a given input state may be described in terms of the scattering

TABLE I. Summary of the special cases examined in the later sections of this paper.

Case no.	No. of photons	Interferometer type	Input state	Frequency correlation
A	1	MZ	Fock	Not applicable
B	1	MZ	N00N	Not applicable
C	2	MZ	Fock	None
D	2	MZ	Dual Fock	None
E	2	MZ	N00N	None
F	2	MZ	Fock	Anticorrelated
G	2	MZ	N00N	Anticorrelated
H	2	MZ	Dual Fock	Anticorrelated
I	1	HOM	N00N	None
J	2	HOM	N00N	None
K	2	HOM	N00N	Anticorrelated
L	2	MZ	SPDC Fock	Anticorrelated

matrix $S(\phi)$. The initial and final annihilation operators are related by a scattering matrix $S(\phi)$:

$$\begin{pmatrix} \hat{c}_\omega(\phi) \\ \hat{d}_\omega(\phi) \end{pmatrix} = S(\phi) \begin{pmatrix} \hat{a}_\omega \\ \hat{b}_\omega \end{pmatrix}, \tag{6}$$

where ϕ is the relative phase difference experienced by photons in the two arms. In the absence of photon losses in the system, the scattering matrix will be unitary. Then, for an ideal Mach-Zehnder interferometer, the scattering matrix is given by

$$\begin{aligned} S(\phi) &= \frac{1}{2}(e^{i\phi}e^{ikL_1} - e^{ikL_2})\sigma_z - \frac{i}{2}(e^{i\phi}e^{ikL_1} + e^{ikL_2})\sigma_x \\ &= -ie^{ikL_1}e^{i\phi/2}\begin{pmatrix} -\sin\frac{\phi}{2} & \cos\frac{\phi}{2} \\ \cos\frac{\phi}{2} & \sin\frac{\phi}{2} \end{pmatrix}, \end{aligned} \tag{7}$$

where the Pauli matrices are

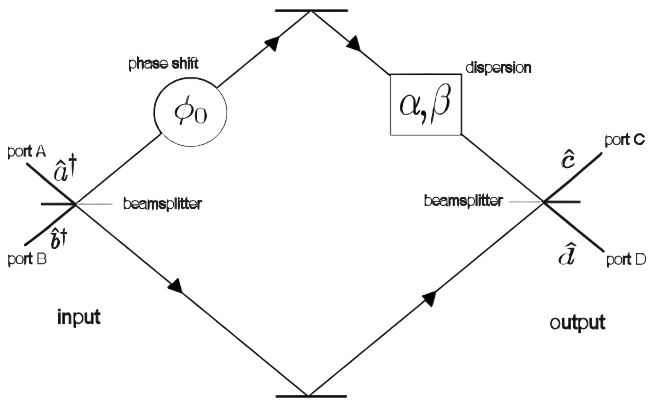

FIG. 1. Mach-Zehnder interferometer with dispersion in one arm. There is also a phase shift ϕ_0 of nondispersive origin in the same arm.

$$\sigma_x = \begin{pmatrix} 0 & 1 \\ 1 & 0 \end{pmatrix} \quad \text{and} \quad \sigma_z = \begin{pmatrix} 1 & 0 \\ 0 & -1 \end{pmatrix}. \tag{8}$$

In this scattering matrix we have assumed (as we will assume henceforth) that the lengths of the two interferometer arms are equal, $L_1 = L_2$. Using this matrix in Eq. (6), we can invert the equation and take adjoints to arrive at the following result:

$$\hat{a}_\omega^\dagger = i\left(\hat{c}_\omega^\dagger \sin\frac{\phi}{2} - \hat{d}_\omega^\dagger \cos\frac{\phi}{2}\right)e^{i\phi/2}, \tag{9}$$

$$\hat{b}_\omega^\dagger = -i\left(\hat{c}_\omega^\dagger \cos\frac{\phi}{2} + \hat{d}_\omega^\dagger \sin\frac{\phi}{2}\right)e^{i\phi/2}. \tag{10}$$

We assume that the frequency distribution for each incoming photon is Gaussian and that each Gaussian has the same width and central frequency, of the form $e^{-\sigma(\omega-\omega_0)^2/2}$. Input and output states will either be states of definite photon number in the sense that they are eigenstates of number operators of the form $\hat{N}_j = \int d\omega\, a_\omega^{(j)\dagger} a_\omega^{(j)}$ (where $a_\omega^{(j)}$ is the annihilation operator for photons at the jth port), or else superpositions of such states.

We introduce dispersion to the upper branch of the interferometer by giving the wave number k a frequency dependence of the form in Eq. (3). We assume that the dispersion in the other branch of the interferometer is negligible, i.e., that $k(\omega) = k_0$ in that branch. The length of the portion of the upper arm for which $k(\omega)$ differs from k_0 will be denoted L, where $0 \leqslant L \leqslant L_1$. In addition to any phase difference resulting from the asymmetric dispersion, we also assume that photons traveling through the upper branch of the interferometer gain an additional phase difference ϕ_0 relative to the lower branch. ϕ_0 is any phase difference of nondispersive origin that may be present in the setup; this may be due to a difference in path length, or an interaction of one arm of the interferometer with an external field. Note that for our setup, the assumption of a balanced interferometer entails no loss of generality; to account for an unbalanced interferometer, it

suffices to simply include a term of the form $k_0(L_1-L_2)$ inside the phase factor ϕ_0.

In the presence of the dispersion, the scattering matrix will now be of the form

$$S(\phi_0) = \frac{1}{2}e^{ik_0L_1}\begin{pmatrix} e^{i\phi(\omega)}-1 & -i(e^{i\phi(\omega)}+1) \\ -i(e^{i\phi(\omega)}+1) & -(e^{i\phi(\omega)}-1) \end{pmatrix} = -ie^{ik_0L_1}e^{i\phi(\omega)/2}\begin{pmatrix} -\sin\frac{\phi(\omega)}{2} & \cos\frac{\phi(\omega)}{2} \\ \cos\frac{\phi(\omega)}{2} & \sin\frac{\phi(\omega)}{2} \end{pmatrix}, \tag{11}$$

where for future convenience we have shifted the frequency dependence into a new phase angle by defining

$$\phi(\omega) = \phi_0 + \alpha L(\omega-\omega_0) + \beta L(\omega-\omega_0)^2. \tag{12}$$

Consider N photons entering the interferometer and assume for now that their frequencies are independent variables. The Fock, dual Fock, and N00N input states are of the form

$$|N,0\rangle_\sigma = \frac{1}{\sqrt{N!}}\left(\frac{\sigma}{\pi}\right)^{N/4}\int d\omega_1\cdots d\omega_N \exp\left(-\frac{\sigma}{2}\sum_{j=1}^{N}(\omega_j-\omega_0)^2\right) \times \hat{a}^\dagger_{\omega_1}\cdots\hat{a}^\dagger_{\omega_N}|0\rangle \tag{13}$$

$$|N,N\rangle_\sigma = \frac{1}{N!}\left(\frac{\sigma}{\pi}\right)^{N/2}\int d\omega_1\cdots d\omega_{2N} \exp\left(-\frac{\sigma}{2}\sum_{j=1}^{2N}(\omega_j-\omega_0)^2\right) \times \hat{a}^\dagger_{\omega_1}\cdots\hat{a}^\dagger_{\omega_N}\hat{b}^\dagger_{\omega_{N+1}}\cdots\hat{b}^\dagger_{\omega_{2N}}|0\rangle \tag{14}$$

and

$$\frac{1}{\sqrt{2}}[|N,0\rangle + |0,N\rangle]_\sigma = \frac{1}{\sqrt{N!}}\frac{1}{\sqrt{2}}\left(\frac{\sigma}{\pi}\right)^{N/4}\int d\omega_1\cdots d\omega_N \times\exp\left(-\frac{\sigma}{2}\sum_{j=1}^{N}(\omega_j-\omega_0)^2\right) \times (\hat{a}^\dagger_{\omega_1}\cdots\hat{a}^\dagger_{\omega_N}+\hat{b}^\dagger_{\omega_1}\cdots\hat{b}^\dagger_{\omega_N})|0\rangle, \tag{15}$$

where the bandwidth of the incident beams is given by $\Delta\omega \equiv \sigma^{-1/2}$. If the photons are produced by SPDC, then the frequencies must occur in pairs with the photons in each pair being equal distances above or below the pump frequency; we will consider this situation in simplified form in Sec. IV B and in a more realistic form in Sec. VII.

Suppose that one of the N-photon or $2N$-photon states described above is input to the interferometer. Write this input state as $|\psi_{in}\rangle$. Then, assuming that the frequencies of the final photons are not measured, we want the joint probabilities to find N_c photons at detector C and N_d photons at detector D (with $N_c+N_d=N_a+N_b$) for a given nondispersive phase shift ϕ_0 in the upper interferometer arm. These probabilities can be expressed in the form

$$P(N_c,N_d|\phi_0) = \langle\psi_{in}|\hat{\pi}(N_c,N_d;\phi_0)|\psi_{in}\rangle, \tag{16}$$

where the projective operator $\hat{\pi}(N_c,N_d;\phi_0)$ is defined as

$$\hat{\pi}(N_c,N_d,\phi_0) = \int d\Omega|N_c,N_d;\Omega,\phi_0\rangle\langle N_c,N_d;\Omega,\phi_0|, \tag{17}$$

with

$$|N_c,N_d;\Omega,\phi_0\rangle = \frac{1}{\sqrt{N_c!N_d!}}\hat{c}^\dagger_{\Omega_1}\cdots\hat{c}^\dagger_{\Omega_{N_c}}\hat{d}^\dagger_{\Omega'_1}\cdots\hat{d}^\dagger_{\Omega'_{N_d}}|0\rangle. \tag{18}$$

Here we have suppressed the ϕ_0 dependence of the $\hat{c}_\Omega$ and $\hat{d}_{\Omega'}$ operators for notational simplicity, and have represented the collection of output frequencies $\{\Omega_1,\ldots,\Omega_{N_c},\Omega'_1,\ldots,\Omega'_{N_d}\}$ by the single symbol Ω. Similarly, $d\Omega$ is being used as shorthand for the full frequency integration measure $d\Omega_1\cdots d\Omega_{N_c}d\Omega'_1\cdots d\Omega'_{N_d}$. These probabilities may also be expressed in the form

$$P(N_c,N_d|\phi_0) = \int d\Omega|\langle N_c,N_d;\Omega,\phi_0|\psi_{in}\rangle|^2. \tag{19}$$

From Eq. (2) the mutual information between the phase Φ and the output photon numbers M is then

$$H(\Phi{:}M) = \frac{1}{2\pi}\sum_{N_c,N_d}\int_{-\pi}^{\pi}d\phi_0 P(N_c,N_d|\phi_0) \times\log_2\left(\frac{2\pi P(N_c,N_d|\phi_0)}{\int_{-\pi}^{\pi}d\phi_0 P(N_c,N_d|\phi_0)}\right). \tag{20}$$

We note that the probabilities $P(N_c,N_d,|\phi_0)$ are also conditional upon the values of α, β, and σ, although we do not explicitly include these parameters in the notation for the probabilities for the sake of notational simplicity. We now restrict ourselves to the cases $N=1$ and 2, and proceed in the following sections to compute the mutual information H for a number of different possible input states.

III. MZ INTERFEROMETRY WITH ONE-PHOTON INPUT

In this section, we begin with the cases in which there is only one photon in the initial state.

Case A: One-photon Fock state. We introduce the normalized input state

$$|\psi_{in}\rangle_\sigma = |10\rangle_\sigma = \sqrt[4]{\frac{\sigma}{\pi}}\int d\omega\, e^{-(\sigma/2)(\omega-\omega_0)^2}\hat{a}^\dagger_\omega|0\rangle, \tag{21}$$

representing a single photon incident on port A. Using relations (9) and (10), this is equivalent to

$$|10\rangle_\sigma = \frac{1}{2}\sqrt[4]{\frac{\sigma}{\pi}}\int d\omega\, e^{-(\sigma/2)(\omega-\omega_0)^2} \times[\hat{c}^\dagger_\omega(e^{i\phi(\omega)}-1) - i\hat{d}^\dagger_\omega(e^{i\phi(\omega)}+1)]|0\rangle. \tag{22}$$

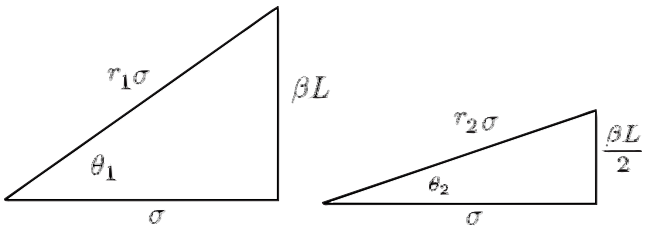

FIG. 2. Definitions of r_1, r_2, θ_1, and θ_2.

The photon may leave the interferometer via either port C or port D. We assume that the detectors count the number of photons leaving the apparatus but do not measure their frequencies. Therefore, we must integrate over the final frequencies. The output state is then measured using the projective operators

$$\hat{\pi}(1,0) = \int d\Omega\, \hat{c}_\Omega^\dagger |0\rangle\langle 0|\hat{c}_\Omega, \tag{23}$$

$$\hat{\pi}(0,1) = \int d\Omega\, \hat{d}_\Omega^\dagger |0\rangle\langle 0|\hat{d}_\Omega. \tag{24}$$

Expectation values of these operators give the probabilities of measurement outcomes:

$$P(1,0|\phi_0) = \frac{1}{2}\left[1 - \frac{e^{-(\alpha^2 L^2/4r_1^2\sigma)}}{\sqrt{r_1}}\cos\left(\phi_0 + \frac{\theta_1}{2} - \frac{\alpha^2\beta L^3}{4r_1^2\sigma^2}\right)\right], \tag{25}$$

$$P(0,1|\phi_0) = \frac{1}{2}\left[1 + \frac{e^{-(\alpha^2 L^2/4r_1^2\sigma)}}{\sqrt{r_1}}\cos\left(\phi_0 + \frac{\theta_1}{2} - \frac{\alpha^2\beta L^3}{4r_1^2\sigma^2}\right)\right]. \tag{26}$$

In the previous two lines, we have introduced some notation that will be convenient for simplifying the results of this and the following sections. The parameters r_1, r_2, θ_1, and θ_2 are defined by

$$r_1^2 = 1 + \left(\frac{\beta L}{\sigma}\right)^2, \quad \tan\theta_1 = \frac{\beta L}{\sigma}, \tag{27}$$

$$r_2^2 = 1 + \left(\frac{\beta L}{2\sigma}\right)^2, \quad \tan\theta_2 = \frac{\beta L}{2\sigma} \tag{28}$$

(see Fig. 2). Note that these parameters depend on the second-order dispersion coefficient β, but not on α, and that when β vanishes we then have $r_1 = r_2 = 1$ and $\theta_1 = \theta_2 = 0$.

Case B: One-photon N00N state. The input state is

$$\frac{1}{\sqrt{2}}[|10\rangle + |01\rangle]_\sigma = \frac{1}{\sqrt{2}}\sqrt[4]{\frac{\sigma}{\pi}}\int d\omega\, e^{-(\sigma/2)(\omega-\omega_0)^2}(\hat{a}_\omega^\dagger + \hat{b}_\omega^\dagger)|0\rangle, \tag{29}$$

where

$$\frac{1}{\sqrt{2}}(\hat{a}_\omega^\dagger + \hat{b}_\omega^\dagger) = \frac{i}{2\sqrt{2}}\{\hat{c}_\omega^\dagger[(i-1) - (i+1)e^{i\phi(\omega)}] + \hat{d}_\omega^\dagger[e^{i\phi(\omega)}(i-1) - (i+1)]\}. \tag{30}$$

The resulting output probabilities in this case turn out to be

$$P(1,0|\phi_0) = \frac{1}{2}\left[1 - \frac{e^{-(\alpha^2\beta L^3/4r_1^2\sigma)}}{\sqrt{r_1}}\sin\left(\phi_0 + \frac{\theta_1}{2} - \frac{\alpha^2\beta L^3}{4r_1^2\sigma^2}\right)\right], \tag{31}$$

$$P(0,1|\phi_0) = \frac{1}{2}\left[1 + \frac{e^{-(\alpha^2\beta L^3/4r_1^2\sigma)}}{\sqrt{r_1}}\sin\left(\phi_0 + \frac{\theta_1}{2} - \frac{\alpha^2\beta L^3}{4r_1^2\sigma^2}\right)\right]. \tag{32}$$

IV. MZ INTERFEROMETRY WITH TWO-PHOTON INPUT

We now consider input states with two photons distributed in assorted ways among the input ports. However, now we must make a distinction as to whether the two photon frequencies are independent or correlated in some manner. We treat the uncorrelated version first. Then we will examine one particular case of frequency-correlated photons which is of special interest for experiment: that of photon pairs created through spontaneous parametric down-conversion. In this section we treat only a simplified version of SPDC which will allow us to obtain simple exact expressions for the probabilities of all of the output states. In a later section we will compare this simplified SPDC to a more realistic version for which only numerical results are available.

A. Two-photon input with uncorrelated energies

Case C: Energy-uncorrelated two-photon Fock state. Sending a two-particle Fock state into input A,

$$|2,0\rangle_\sigma = \sqrt{\frac{\sigma}{2\pi}}\int d\omega_1 d\omega_2 e^{-(\sigma/2)[(\omega_1-\omega_0)^2+(\omega_2-\omega_0)^2]}\hat{a}_{\omega_1}^\dagger\hat{a}_{\omega_2}^\dagger|0\rangle, \tag{33}$$

where we use Eqs. (9) and (10) to write each $\hat{a}^\dagger$ factor in terms of the output operators $\hat{c}^\dagger$ and $\hat{d}^\dagger$. After a straightforward calculation, this leads to the following output probabilities:

$$P(2,0|\phi_0) = \frac{1}{4}\left[1 - \frac{e^{-(\alpha^2 L^2/4r_1^2\sigma)}}{\sqrt{r_1}}\cos\left(\phi_0 + \frac{\theta_1}{2} - \frac{\alpha^2\beta L^3}{4r_1^2\sigma^2}\right)\right]^2, \tag{34}$$

$$P(0,2|\phi_0) = \frac{1}{4}\left[1 + \frac{e^{-(\alpha^2 L^2/4r_1^2\sigma)}}{\sqrt{r_1}}\cos\left(\phi_0 + \frac{\theta_1}{2} - \frac{\alpha^2\beta L^3}{4r_1^2\sigma^2}\right)\right]^2, \tag{35}$$

$$P(1,1|\phi_0) = \frac{1}{2}\left[1 - \frac{e^{-(\alpha^2 L^2/2r_1^2\sigma)}}{r_1}\cos^2\left(\phi_0 + \frac{\theta_1}{2} - \frac{\alpha^2\beta L^3}{4r_1^2\sigma^2}\right)\right]. \tag{36}$$

Case D: Energy-uncorrelated two-photon dual Fock input. The normalized input state is

$$|1,1\rangle_\sigma = \sqrt{\frac{\sigma}{\pi}} \int d\omega_1 \omega_2 e^{-(\sigma/2)[(\omega_1-\omega_0)^2+(\omega_2-\omega_0)^2]} \hat{a}^\dagger_{\omega_1} \hat{a}^\dagger_{\omega_2} |0\rangle \tag{37}$$

$$\begin{aligned} &= \frac{1}{4}\sqrt{\frac{\sigma}{\pi}} \int d\omega_1 \omega_2 e^{-(\sigma/2)[(\omega_1-\omega_0)^2+(\omega_2-\omega_0)^2]} \\ &\times [-i\hat{c}^\dagger_{\omega_1}\hat{c}^\dagger_{\omega_2}(e^{i\phi(\omega_1)}-1)(e^{i\phi(\omega_2)}+1) \\ &+ i\hat{d}^\dagger_{\omega_1}\hat{d}^\dagger_{\omega_2}(e^{i\phi(\omega_2)}-1)(e^{i\phi(\omega_1)}+1) \\ &+ \hat{c}^\dagger_{\omega_1}\hat{d}^\dagger_{\omega_2}(e^{i\phi(\omega_1)}-1)(e^{i\phi(\omega_2)}-1) \\ &- \hat{c}^\dagger_{\omega_2}\hat{d}^\dagger_{\omega_1}(e^{i\phi(\omega_1)}+1)(e^{i\phi(\omega_2)}+1)]|0\rangle, \end{aligned} \tag{38}$$

which gives the results

$$\begin{aligned} P(2,0) &= P(0,2) \\ &= \frac{1}{4}\left[1 - \frac{e^{-(\alpha^2L^2/2r_1^2\sigma)}}{r_1}\cos\left(2\phi_0 + \theta_1 - \frac{\alpha^2\beta L^3}{2r_1^2\sigma^2}\right)\right], \end{aligned} \tag{39}$$

$$P(1,1) = \frac{1}{2}\left[1 + \frac{e^{-(\alpha^2L^2/2r_1^2\sigma)}}{r_1}\cos\left(2\phi_0 + \theta_1 - \frac{\alpha^2\beta L^3}{2r_1^2\sigma^2}\right)\right]. \tag{40}$$

Case E: Energy-uncorrelated two-photon N00N state. For the input state

$$\begin{aligned} |20\rangle_\sigma + |02\rangle_\sigma &= \sqrt{\frac{\sigma}{2\pi}} \int d\omega_1 d\omega_2 e^{-(\sigma/2)[(\omega_1-\omega_0)^2+(\omega_2-\omega_0)^2]} \\ &\times \frac{1}{\sqrt{2}}(\hat{a}^\dagger_{\omega_1}\hat{a}^\dagger_{\omega_2} + \hat{b}^\dagger_{\omega_1}\hat{b}^\dagger_{\omega_2})|0\rangle, \end{aligned} \tag{41}$$

the output probabilities are

$$P(2,0|\phi_0) = P(0,2|\phi_0) = \frac{1}{4}\left(1 + \frac{1}{r_1}e^{-(\alpha^2L^2/2r_1^2\sigma)}\right), \tag{42}$$

$$P(1,1|\phi_0) = \frac{1}{2}\left(1 - \frac{1}{r_1}e^{-(\alpha^2L^2/2r_1^2\sigma)}\right). \tag{43}$$

In the absence of dispersion ($\alpha=\beta=0$) or in the narrow-bandwidth limit ($\sigma\to\infty$), we see that the coincidence rate $P(1,1|\phi_0)$ vanishes, while the other two probabilities are both equal to $1/2$.

Note that there is no dependence on ϕ_0. We will see later that this fact manifests itself in a vanishing mutual information.

B. Two-photon input with anticorrelated energies: simplified SPDC model

Case F: Simplified SPDC Fock states. We now examine a case with two photons incident on the same input port and anticorrelated in energy. We do this in the context of a simplified model of spontaneous parametric down-conversion. Energy conservation requires that the two down-converted photons have frequencies $\omega_\pm = \omega_0 \pm \Omega$, where $2\omega_0$ is the pump frequency. We again assume a Gaussian distribution of frequencies, centered around ω_0, of the form $e^{-\sigma(\omega_\pm-\omega_0)^2/2} = e^{-(\sigma/2)\Omega^2}$. We follow essentially the same calculational procedure as before, except now we enforce the requirement that the incoming photon frequencies satisfy $\omega_1+\omega_2=2\omega_0$. In this section we impose this condition in a manner that will allow us to obtain analytic solutions for the output probabilities. This will serve us as a simplified version of SPDC, and we will see in Sec. VII that this model seems to give an upper bound to the mutual information obtained from a more realistic model of SPDC. The input state in this model is taken to be of the form

$$|20\rangle_\sigma = \sqrt[4]{\frac{2\sigma}{\pi}} \int_{-\infty}^{\infty} d\Omega \int_{-\infty}^{\infty} d\epsilon\, e^{-\sigma\Omega^2} f(\epsilon) a^\dagger_{\omega_+} a^\dagger_{\omega_-} |0\rangle, \tag{44}$$

where now $\omega_+ = \omega_0+\Omega$ and $\omega_- = \omega_0-\Omega+\epsilon$. We can choose $f(\epsilon)$ to be any function sharply peaked at zero with normalized integral (unit area under its graph). We then compute the output probabilities according to

$$P(N_c,N_d|\phi_0) = \int d\omega_1 d\omega_2 |\langle N_c,N_d|\psi_{in}\rangle|^2, \tag{45}$$

or equivalently, by applying the projection operators

$$\hat{\pi}(N_c,N_d) = \int d\omega_1 d\omega_2 |N_c,N_d\rangle\langle N_c,N_d|. \tag{46}$$

The auxiliary function $f_\lambda(\epsilon)$ is necessary in this model in order to impose the constraint $\omega_1+\omega_2=2\omega_0$ without causing squares of δ functions to arise in the probability calculations. A more correct treatment of SPDC will follow in Sec. VII.

The measurement outcomes, integrated over final frequency, are then given by

$$\begin{aligned} P(2,0|\phi_0) = \frac{1}{8}\Bigg\{ &2 + e^{-(\alpha^2L^2/2\sigma)} + \frac{1}{\sqrt{r_1}}\cos\left(2\phi_0 + \frac{\theta_1}{2}\right) \\ &- \frac{4}{\sqrt{r_2}}e^{-(\alpha^2L^2/8r_2^2\sigma)}\cos\left[\phi_0 + \frac{\theta_2}{2} - \frac{\alpha^2\beta L^3}{16r_2^2\sigma^2}\right]\Bigg\}, \end{aligned} \tag{47}$$

$$\begin{aligned} P(0,2|\phi_0) = \frac{1}{8}\Bigg\{ &2 + e^{-(\alpha^2L^2/2\sigma)} + \frac{1}{\sqrt{r_1}}\cos\left(2\phi_0 + \frac{\theta_1}{2}\right) \\ &+ \frac{4}{\sqrt{r_2}}e^{-(\alpha^2L^2/8r_2^2\sigma)}\cos\left[\phi_0 + \frac{\theta_2}{2} - \frac{\alpha^2\beta L^3}{16r_2^2\sigma^2}\right]\Bigg\}, \end{aligned} \tag{48}$$

$$P(1,1|\phi_0) = \frac{1}{4}\left[2 - e^{-(\alpha^2 L^2/2\sigma)} - \frac{1}{\sqrt{r_1}}\cos\left(2\phi_0 + \frac{\theta_1}{2}\right)\right]. \tag{49}$$

As β increases, r_1 and r_2 increase, leading to decreased visibility of all of the oscillating terms.

Note also that in the case of zero dispersion ($\alpha=\beta=0$) the exact expressions for energy-uncorrelated (case C, Sec. IV A) and energy-anticorrelated (down-converted) Fock states (case F) are identical to each other. However, the probabilities begin to diverge when dispersion is turned on. The same effect will be seen to occur for the uncorrelated and anticorrelated N00N states in the HOM interferometer (cases J and K, below).

Case G: Simplified SPDC N00N states. Now the input state is taken to be a N00N state, $(1/\sqrt{2})\{|20\rangle_{\lambda,\sigma}+|02\rangle_{\lambda,\sigma}\}$. We find the measurement outcomes to be

$$P(2,0|\phi_0) = P(2,0|\phi_0) = \frac{1}{4}(1 + e^{-(\alpha^2 L^2/2\sigma)}), \tag{50}$$

$$P(1,1|\phi_0) = \frac{1}{2}(1 - e^{-(\alpha^2 L^2/2\sigma)}). \tag{51}$$

As in the uncorrelated case, the probabilities show no dependence on ϕ_0, and so have vanishing mutual information. In this case we also see that there is no dependence on the second-order dispersion coefficient β.

It is interesting to note what happens if we shift the phase of the photons in one input port by $\pi/2$ before they hit the first beam splitter. The input to the interferometer is now proportional to $|2,0\rangle - |0,2\rangle$. In this case, the interference in ϕ_0 reemerges, and the result is independent of α instead of β. In fact, the counting probabilities turn out to be very similar to those of the N00N state incident on a HOM interferometer presented in the next section (case K). Moreover, these two cases have identical values for the mutual information.

Case H: Simplified SPDC dual Fock state

The frequency-anticorrelated dual Fock input state

$$|1,1\rangle_\sigma = \sqrt[4]{\frac{\sigma}{2\pi}} \int d\Omega \int d\epsilon\, e^{-\sigma\Omega^2} f(\epsilon) \hat{a}^\dagger_{\omega_+} \hat{b}^\dagger_{\omega_-} |0\rangle \tag{52}$$

gives the results

$$P(2,0|\phi_0) = P(0,2|\phi_0) = \frac{1}{4}\left[1 - \frac{1}{\sqrt{r_1}}\cos\left(2\phi_0 + \frac{\theta_1}{2}\right)\right], \tag{53}$$

$$P(1,1|\phi_0) = \frac{1}{2}\left[1 + \frac{1}{\sqrt{r_1}}\cos\left(2\phi_0 + \frac{\theta_1}{2}\right)\right]. \tag{54}$$

V. DISPERSIVE HONG-OU-MANDEL INTERFEROMETER WITH N00N INPUT

An alternative setup has been proposed to improve phase resolution [6]. In this section we examine this alternate version and compare it to the previous results.

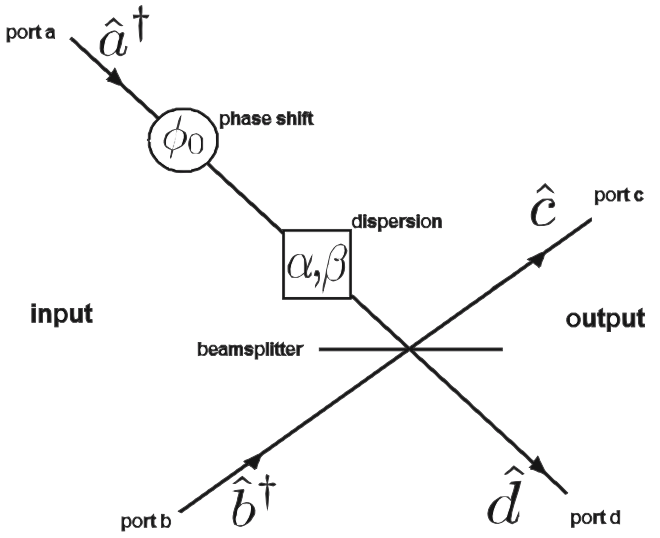

FIG. 3. Hong-Ou-Mandel interferometer with dispersion and nondispersive phase shift ϕ_0 in one arm.

In this version, it is assumed that the N00N state is created *inside* the interferometer, rather than at the input ports. Effectively, we need to remove the first beam splitter from the interferometer and use the N00N state as input to the remaining beamsplitter, which now acts as a Hong-Ou-Mandel interferometer [13]. The setup is shown in Fig. 3. We again assume dispersion and phase-shift ϕ_0 along one of the lines entering the beam splitter, neglecting absorption. Ignoring an overall constant phase of $e^{ik_0 L}$, the scattering matrix now has the form

$$S(\phi_0) = \frac{1}{\sqrt{2}}\begin{pmatrix} e^{i\phi(\omega)} & i \\ ie^{i\phi(\omega)} & +1 \end{pmatrix}, \tag{55}$$

where $\phi(\omega)$ is again given by Eq. (12). Thus,

$$\hat{c}_\omega = \frac{1}{\sqrt{2}}(e^{i\phi(\omega)}\hat{a}_\omega + i\hat{b}_\omega), \tag{56}$$

$$\hat{d}_\omega = \frac{1}{\sqrt{2}}(ie^{i\phi(\omega)}\hat{a}_\omega + \hat{b}_\omega). \tag{57}$$

Case I: Single-photon N00N state in HOM interferometer. By the same methods as before, we can compute the counting rates for a given N00N state input. The one-photon N00N input state is

$$|\psi\rangle = C \int d\omega\, e^{-(\sigma/2)(\omega-\omega_0)^2}(a^\dagger_\omega + b^\dagger_\omega)|0\rangle, \tag{58}$$

for which we find

$$P(1,0|\phi_0) = \frac{1}{2}\left[1 + \frac{e^{-(\alpha^2 L^2/4r_1^2\sigma)}}{\sqrt{r_1}}\sin\left(\phi_0 + \frac{\theta_1}{2} - \frac{\alpha^2\beta L^3}{4r_1^2\sigma^2}\right)\right], \tag{59}$$

$$P(0,1|\phi_0) = \frac{1}{2}\left[1 - \frac{e^{-(\alpha^2 L^2/4r_1^2\sigma)}}{\sqrt{r_1}} \sin\left(\phi_0 + \frac{\theta_1}{2} - \frac{\alpha^2\beta L^3}{4r_1^2\sigma^2}\right)\right]. \tag{60}$$

Finally, assuming two-photons, with no correlation or with anticorrelation, we arrive at two additional cases (J and K).

Case J: Energy-uncorrelated two-photon N00N state in HOM interferometer. The input state is

$$|\psi\rangle = C\int d\omega_1 d\omega_2 e^{-(\sigma/2)[(\omega_1-\omega_0)^2+(\omega_2-\omega_0)^2]} \times (a^\dagger_{\omega_1}a^\dagger_{\omega_2} + b^\dagger_{\omega_1}b^\dagger_{\omega_2})|0\rangle. \tag{61}$$

From this state, we arrive at the results

$$P(2,0|\phi_0) = P(0,2|\phi_0) = \frac{1}{4}\left[1 - \frac{e^{-(\alpha^2 L^2/2r_1^2\sigma)}}{r_1}\cos\left(2\phi_0 + \theta_1 - \frac{\alpha^2\beta L^3}{2r_1^2\sigma^2}\right)\right], \tag{62}$$

$$P(1,1|\phi_0) = \frac{1}{2}\left[1 + \frac{e^{-(\alpha^2 L^2/2r_1^2\sigma)}}{r_1}\cos\left(2\phi_0 + \theta_1 - \frac{\alpha^2\beta L^3}{2r_1^2\sigma^2}\right)\right]. \tag{63}$$

Case K: Simplified SPDC two-photon N00N state in HOM interferometer. For the input

$$|\psi\rangle = C\int d\Omega\, e^{-\sigma\Omega^2}(a^\dagger_{\omega_+}a^\dagger_{\omega_-} + b^\dagger_{\omega_+}b^\dagger_{\omega_-})|0\rangle, \tag{64}$$

we compute

$$P(2,0|\phi_0) = P(0,2|\phi_0) = \frac{1}{4}\left[1 - \frac{1}{\sqrt{r_1}}\cos\left(2\phi_0 + \frac{\theta_1}{2}\right)\right], \tag{65}$$

$$P(1,1|\phi_0) = \frac{1}{2}\left[1 + \frac{1}{\sqrt{r_1}}\cos\left(2\phi_0 + \frac{\theta_1}{2}\right)\right]. \tag{66}$$

In this last case, the results turn out to be independent of the first order dispersion coefficient, α.

VI. COMPARISON AND DISCUSSION OF CASES A TO K

The detection probabilities of the previous sections can now be combined with Eq. (2) to compute the mutual information for each of the experimental setups and input states. Plotting the results as functions of α, β, and σ, we find the results in Figs. 4–6 for single-photon input and Figs. 7–9 for two photons. αL is given in units of ω_0^{-1}, while βL and σ are in units of ω_0^{-2}. In the dispersionless limit, $\alpha,\beta\to 0$, we find Shannon mutual information values that agree with those previously calculated in [9].

Only positive values of β were graphed. However, the formulas of the previous sections work equally in the anomalous dispersion (negative β) region.

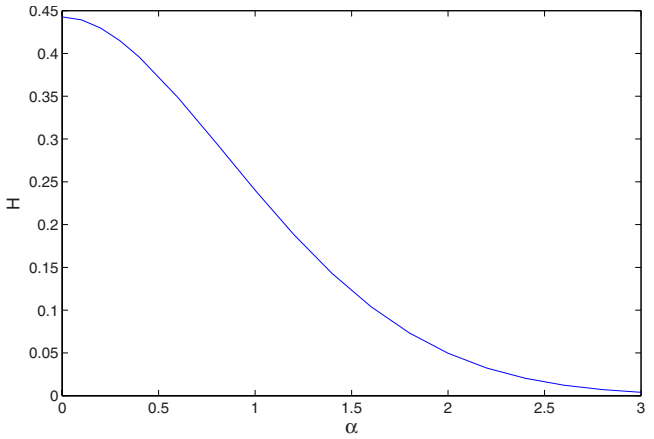

FIG. 4. (Color online) Mutual information versus α for single-photon cases (cases A, B, and I), plotted for the values $\beta=0$, $\sigma=1$. The mutual information is the same for all three cases. (α, β, and σ are in units of $L^{-1}\omega_0^{-1}$, $L^{-1}\omega_0^{-2}$, and ω_0^{-2}, respectively.)

Note also that the four parameters α,β,σ,L appear in all equations only through the dimensionless quantities

$$\Lambda_1 = \frac{\sigma}{\beta L} \quad \text{and} \quad \Lambda_2 = \frac{\sigma}{\alpha^2 L^2}. \tag{67}$$

Thus, other parameter ranges can easily be obtained from those graphed here via appropriate rescaling of variables with the dimensionless ratios held fixed.

A few conclusions are immediately clear from these graphs and from the equations of the previous sections. (i) First, the dual Fock states entering the Mach-Zehnder interferometer give identical results as the N00N states entering the Hong-Ou Mandel interferometer [compare Eqs. (53) and (54) to (65) and (66), or compare Eqs. (39) and (40) to (62) and (63)]. This is to be expected, since for $N=2$ the two cases are equivalent: the first beam splitter in the Mach-Zehnder interferometer turns a dual Fock input state into a N00N output state, which then strikes the second beam splitter. The second beam splitter can then be viewed as a HOM

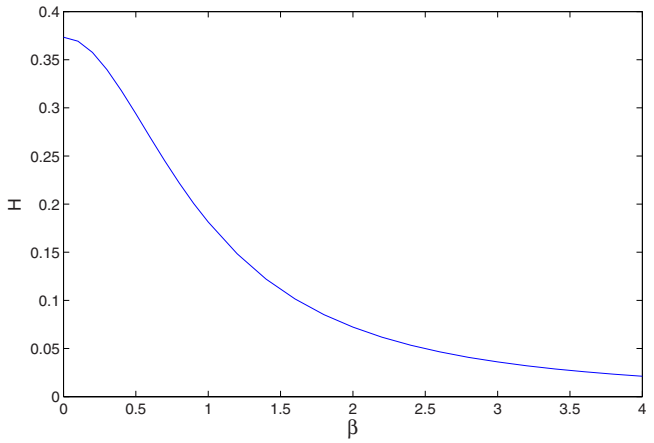

FIG. 5. (Color online) Mutual information versus β for single-photon cases (cases A, B, and I), for the values $\alpha=0.5$, $\sigma=1$. (α, β, and σ are in units of $L^{-1}\omega_0^{-1}$, $L^{-1}\omega_0^{-2}$, and ω_0^{-2}, respectively.)

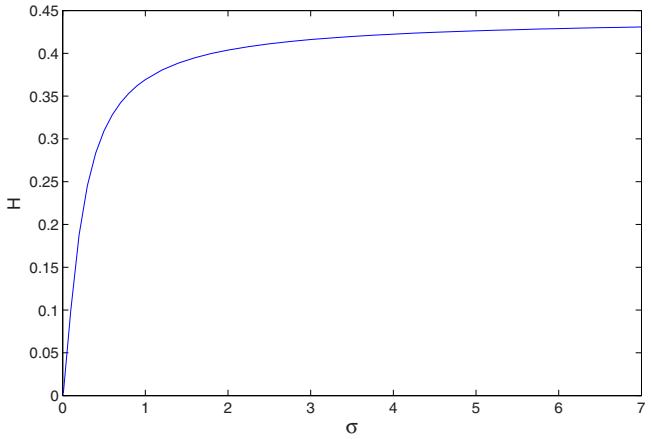

FIG. 6. (Color online) Mutual information versus squared inverse bandwidth σ for single-photon cases (cases A, B, and I), for the values $\alpha=1$, $\beta=0.1$. (α, β, and σ are in units of $L^{-1}\omega_0^{-1}$, $L^{-1}\omega_0^{-2}$, and ω_0^{-2}, respectively.)

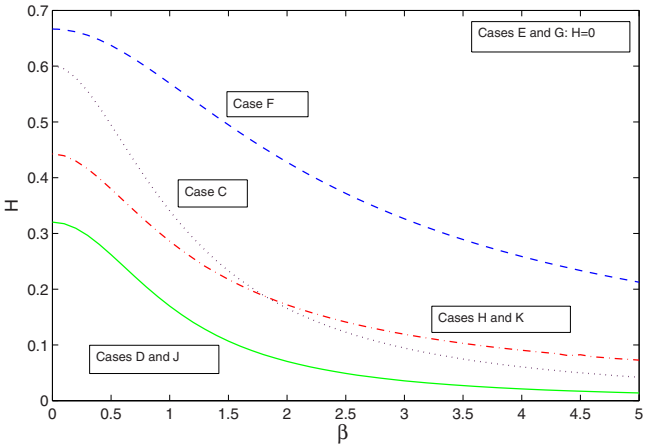

FIG. 8. (Color online) Mutual information versus β for two-photon cases, for the values $\sigma=1$, $\alpha=0.5$. (α, β, and σ are in units of $L^{-1}\omega_0^{-1}$, $L^{-1}\omega_0^{-2}$, and ω_0^{-2}, respectively.)

interferometer. Thus cases J and D are equivalent, as are cases H and K. (This equivalence will not hold for $N>2$.) (ii) Second, the single-photon cases (cases A, B, and I) all give identical curves for the mutual information as functions of α, β, and σ. The explanation for this is clear if the action of the first beam splitter on the input is examined. Cases B and I are equivalent for the same reason mentioned in the previous point: they both lead to a one-particle N00N state in the portion of the interferometer before the dispersive element is reached, and so give the same output. Meanwhile, in case A, the output of the first beam splitter is the state $(1/\sqrt{2})(|01\rangle+i|10\rangle)$; this is similar to a N00N state, except one term is shifted in phase by $\pi/2$ relative to the other. This converts the sines in the probabilities of cases B and I into the cosines of case A [Eqs. (25) and (26)], but has no other effect. Since the mutual information involves integrals from $-\pi$ to π, interchanging sines and cosines inside the integrals has no effect on the mutual information. Unsurprisingly, the single photon cases generally result in lower mutual information than the two-photon cases. (iii) We see from the graphs for the two-photon states that the energy-uncorrelated and energy-anticorrelated version of each input give identical results for zero dispersion or zero bandwidth ($\sigma=\infty$); however, the uncorrelated versions all drop off rapidly to zero fidelity as the dispersion increases, whereas the anticorrelated (downconverted) input leads to a much slower drop. (iv) Two-photon N00N states incident on the MZ interferometer (cases E and G) have zero mutual information as anticipated earlier. (v) For fixed bandwidth and fixed quadratic dispersion coefficient β, the two-photon downconverted N00N state in the HOM interferometer (case K) is independent of the linear coefficient α. However, it decays rapidly with increasing β. (vi) Overall, the simplified SPDC-generated Fock states (case F) seem to hold up best in the presence of dispersion. This case starts off with a higher value of H at zero dispersion and decays more slowly as α and β increase. The only exception to this statement is when β is small, in which case the anticorrelated HOM N00N state (case K) works better at large α.

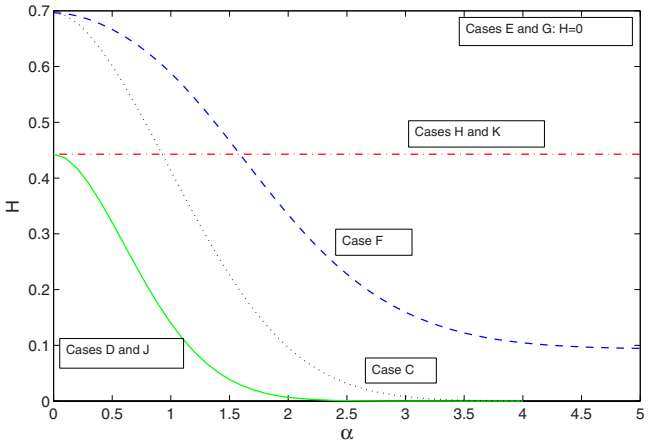

FIG. 7. (Color online). Mutual information versus α for two-photon cases, for the values $\sigma=1$, $\beta=0$. Cases E and G vanish identically. Cases J and D are identical, as are cases H and K. (α, β, and σ are in units of $L^{-1}\omega_0^{-1}$, $L^{-1}\omega_0^{-2}$, and ω_0^{-2}, respectively.)

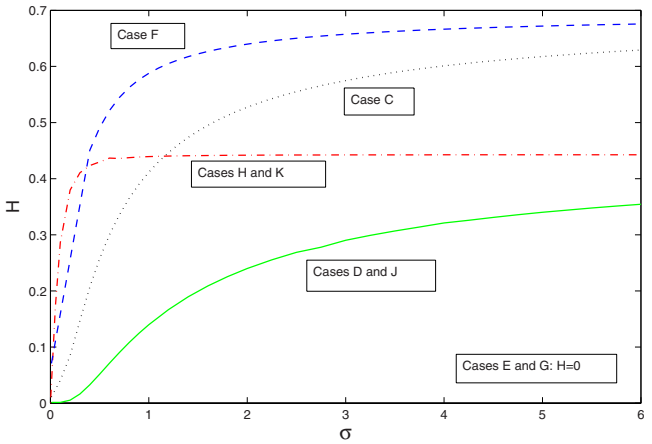

FIG. 9. (Color online) Mutual information versus squared inverse bandwidth σ for two-photon cases, for the values $\alpha=1$, $\beta=0.1$. (α, β, and σ are in units of $L^{-1}\omega_0^{-1}$, $L^{-1}\omega_0^{-2}$, and ω_0^{-2}, respectively.)

A bit of insight into some of the properties of the 2-photon results may be obtained by considering the exponential decay factor

$$\zeta \equiv e^{-(\alpha^2 L^2/4r_1^2\sigma)} = e^{-(\Lambda_2/4r_1^2)} = e^{-[\Lambda_2/4(1+\Lambda_1^{-2})]}. \quad (68)$$

Λ_1 and Λ_2 are the dimensionless quantities defined in Eq. (67). In frequency-uncorrelated cases such as cases C and D, all of the ϕ_0-dependent terms are multiplied by a factor of ζ which arises from interference between $e^{i\phi(\omega_1)}$ and $e^{i\phi(\omega_2)}$ terms, where ω_1 and ω_2 are the frequencies of the photons entering the input ports. The relevant term is of the form $e^{i[\phi(\omega_1)+\phi(\omega_2)]}$. As $\alpha \to \infty$ or $\sigma \to 0$, we find that $\Lambda_2 \to 0$ and $\zeta \to 0$, so that only constant (ϕ_0-independent) terms survive in the limit. Thus, for large α or small σ, the dependence of the probability distributions on ϕ_0 decays exponentially, causing the mutual information to also decay rapidly.

In contrast, for the frequency-anticorrelated cases, such as F and H, the term $e^{i(\phi(\omega_1)+\phi(\omega_2))}$ becomes

$$e^{i[\phi(\omega_+)+\phi(\omega_-)]} = e^{i[2\phi_0+2\beta\omega^2]}, \quad (69)$$

with the α dependence canceling. As a result, ϕ_0-dependent terms occur without the exponentially decaying ζ factor, allowing much slower decay of H at large α (or even no decay at all, as in case H). The slower decay at large dispersion is therefore a direct consequence of the quantum-mechanical correlations present in the initial state.

As for the β dependence, we see that as β becomes large, both ζ and r_1 become β independent, with $\zeta \to e^{-(\Lambda_2/4)}$ and $r_1 \to 1$; thus all the curves approach constant values at large β, with slopes $dH/d\beta$ of comparable order of magnitude.

We turn now to one additional case, that of more realistic SPDC photon pairs, which we then proceed to compare with the simplified SPDC model already examined.

VII. CASE L: SPDC

Now we present results for the mutual information using a more realistic model for the parametric downconversion process. Numerically, the results turn out qualitatively (and for some parameter ranges quantitatively as well) to be very similar to those of the simplified SPDC model in the previous section; however we no longer will be able to present explicit analytic expressions for the measurement outcomes.

There are many possible cases that could be considered, but we restrict ourselves here to the single case of collinear type-II SPDC in a nonlinear crystal, with both of the outgoing photons entering port A of the dispersive Mach-Zehnder interferometer. We now have to consider the parameters of both the interferometer and the crystal. We allow the pump frequency to vary around central frequency $2\omega_0$, with the deviation from the center of the distribution represented by $2\Omega_p$; in other words, the pump frequency is represented as

$$\omega_p = 2(\omega_0 + \Omega_p).$$

We once again assume a Gaussian distribution of frequencies, in this case represented by a weighting factor $e^{-(\sigma/2)(\omega_p-2\omega_0)^2} = e^{-2\sigma\Omega_p^2}$. The signal and idler frequencies are then

$$\omega_s = \frac{\omega_p}{2} + \Omega = \omega_0 + \Omega_p + \Omega, \quad (70)$$

$$\omega_i = \frac{\omega_p}{2} - \Omega = \omega_0 + \Omega_p - \Omega, \quad (71)$$

with $\omega_s + \omega_i = \omega_p$. Suppose that the crystal is cut so that exact phase matching occurs at the central frequency

$$k_p(2\omega_0) = k_s(\omega_0) + k_i(\omega_0). \quad (72)$$

Then, assuming that terms quadratic and higher in the frequencies are small, the phase matching condition for the crystal gives us a condition on the wave vectors of the form [14]

$$\Delta k \equiv k_p(\omega_p) - k_s(\omega_s) - k_i(\omega_i) = \Lambda_p \Omega_p + \Lambda\Omega, \quad (73)$$

where $\Lambda_p = 2k_p'(2\omega_0) - k_s'(\omega_0) - k_i'(\omega_0)$ and $\Lambda = k_i'(\omega_0) - k_s'(\omega_0)$.

The wave function for the biphoton state entering the interferometer is now

$$|\psi_{in}\rangle = \int d\Omega\, d\Omega_p \Phi(\Omega_p, \Omega) \hat{a}^\dagger_{\omega_0+\Omega_p+\Omega} \hat{a}^\dagger_{\omega_0+\Omega_p-\Omega} |0\rangle, \quad (74)$$

where

$$\Phi(\Omega_p, \Omega) = \mathcal{N} e^{-2\sigma\Omega_p^2} \left(\frac{\sin \frac{\Delta k L_c}{2}}{\frac{\Delta k L_c}{2}} \right) e^{-i\Delta k L_c/2}, \quad (75)$$

with normalization constant $\mathcal{N}$. Here, L_c is the length of the nonlinear crystal. Using this wave function, we can compute output probabilities as before. Denoting the frequencies at the detectors by ω and ω', we have

$$P(2,0|\phi_0) = \int d\omega\, d\omega' \left| \Phi\left(\frac{\omega-\omega'}{2}, \omega_0 - \frac{\omega+\omega'}{2} \right) + \Phi\left(-\frac{\omega-\omega'}{2}, \omega_0 - \frac{\omega+\omega'}{2} \right) \right|^2 \times \left| 1 + e^{i[\phi(\omega)+\phi(\omega')]} - e^{i\phi(\omega)} - e^{i\phi(\omega')} \right|^2, \quad (76)$$

$$P(1,1|\phi_0) = \int d\omega\, d\omega' \left| \Phi\left(\frac{\omega-\omega'}{2}, \omega_0 - \frac{\omega+\omega'}{2} \right) \times [1 - e^{i[\phi(\omega)+\phi(\omega')]} - e^{i\phi(\omega)} + e^{i\phi(\omega')}] + \Phi\left(\frac{\omega-\omega'}{2}, \omega_0 - \frac{\omega+\omega'}{2} \right) \times [1 - e^{i[\phi(\omega)+\phi(\omega')]} + e^{i\phi(\omega)} - e^{i\phi(\omega')}] \right|^2, \quad (77)$$

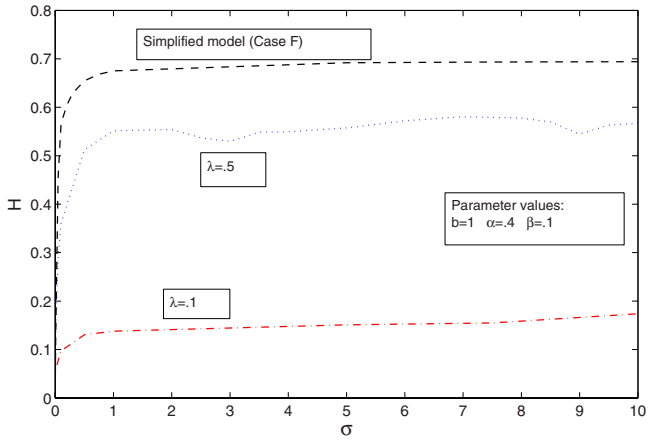

FIG. 10. (Color online) Mutual information versus squared inverse bandwidth σ for SPDC. (α, β, and σ are in units of $L^{-1}\omega_0^{-1}$, $L^{-1}\omega_0^{-2}$, and ω_0^{-2}, respectively. b is in units of ω_0^{-2}, while λ is dimensionless.)

$$P(0,2|\phi_0) = \int d\omega\, d\omega' \left| \Phi\left(\frac{\omega-\omega'}{2}, \omega_0 - \frac{\omega+\omega'}{2}\right) + \Phi\left(-\frac{\omega-\omega'}{2}, \omega_0 - \frac{\omega+\omega'}{2}\right)\right|^2 \times \left|1 + e^{i[\phi(\omega)+\phi(\omega')]} + e^{i\phi(\omega)} + e^{i\phi(\omega')}\right|^2, \tag{78}$$

where $\phi(\omega)$ is as defined in Eq. (12). Note that $\Phi((\omega-\omega')/2, \omega_0-(\omega+\omega')/2)$ depends only on the crystal properties, while $\phi(\omega)$ depends only on the properties of the interferometer. The integrands of $P(0,2|\phi_0)$ and $P(2,0|\phi_0)$ factor in their dependence on these two sets of parameters; that of $P(1,1|\phi_0)$ does not, indicating the entangled nature of the $|11\rangle$ state.

Given these output probabilities, the mutual information can once again be computed. In contrast to the previous sections, the analytic forms of the probabilities are too complicated to be enlightening, so we proceed to numerical calculations. Some examples are graphed in Figs. 10–14. The plots are expressed in terms of the new parameters $b=\Lambda_p L_c$ and $\lambda=\Lambda/\Lambda_p$.

Examples of the dependence of H on the parameters of the pump beam (σ), interferometer (α, β), and nonlinear crystal (λ, b) are given in Figs. 10–14. We see that, although H decays overall with increasing values of the dispersion parameters in the interferometer, α and β, there are oscillations superimposed on the decay, which are especially noticeable at low values of α and β. This effect was in fact also present in the simplified SPDC model of the previous sections, but in the latter case the oscillations were too weak to be visible on the graphs. We see also that as either b or λ increases (or equivalently, as Λ or Λ_p increases), the plots approach those of the simplified SPDC model. Since Λ and b are proportional to the crystal length, this means that the simplified SPDC model is an increasingly better approximation to real SPDC for longer crystals. It also appears from the numerical simulations that for a given set of parameter values α, β, L, and σ, the simplified SPDC model provides an upper bound to H for the real SPDC cases with the same parameter values. The maximum information content clearly

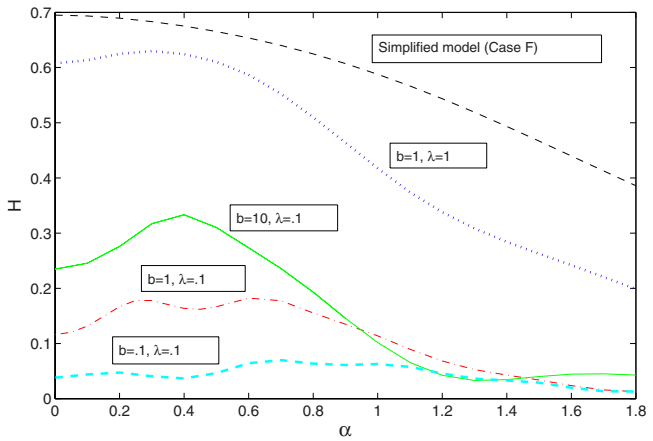

FIG. 11. (Color online) Mutual information versus α for SPDC with $\sigma=1$, $\beta=0.1$. (α, β, and σ are in units of $L^{-1}\omega_0^{-1}$, $L^{-1}\omega_0^{-2}$, and ω_0^{-2}, respectively. b is in units of ω_0^{-2}, while λ is dimensionless.)

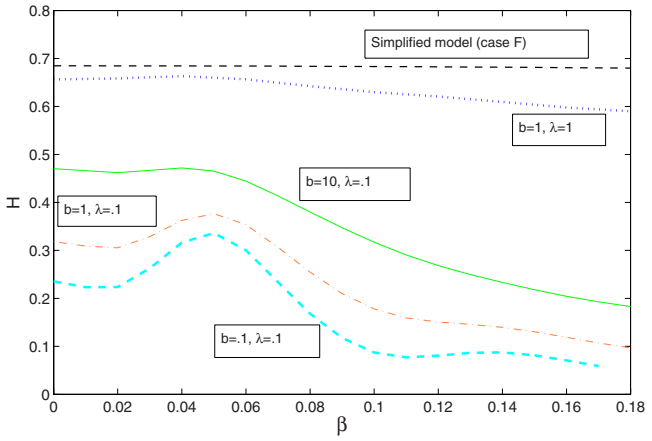

FIG. 12. (Color online) Mutual information versus β for SPDC with $\sigma=1$, $\alpha=0.3$. (α, β, and σ are in units of $L^{-1}\omega_0^{-1}$, $L^{-1}\omega_0^{-2}$, and ω_0^{-2}, respectively. b is in units of ω_0^{-2}, while λ is dimensionless.)

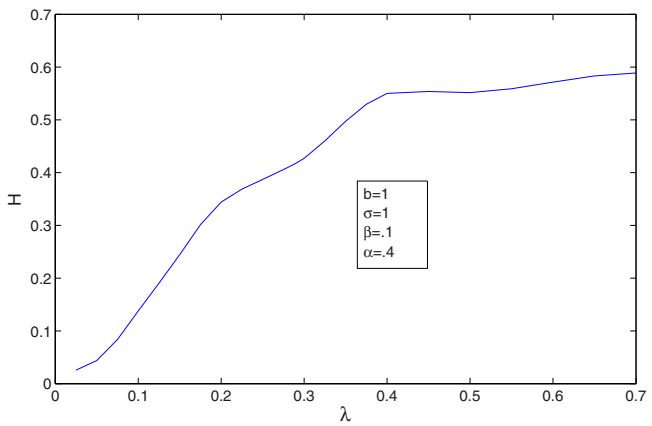

FIG. 13. (Color online) Mutual information versus $\lambda=\Lambda/\Lambda_p$ for SPDC. (α, β, and σ are in units of $L^{-1}\omega_0^{-1}$, $L^{-1}\omega_0^{-2}$, and ω_0^{-2}, respectively. b is in units of ω_0^{-2}, while λ is dimensionless.)

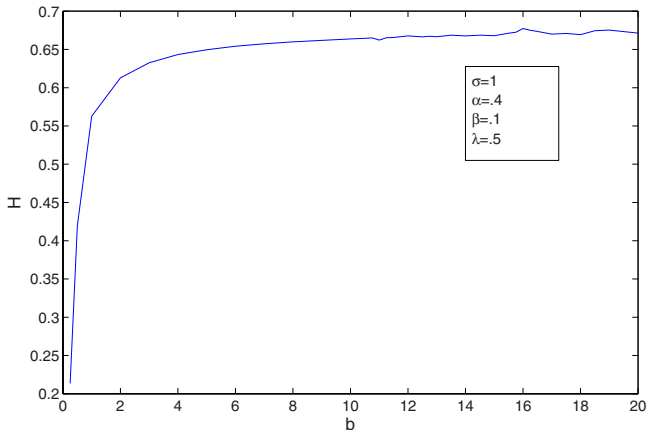

FIG. 14. (Color online) Mutual information versus $b=(L_c/2)\Lambda_p$ for SPDC. (α, β, and σ are in units of $L^{-1}\omega_0^{-1}$, $L^{-1}\omega_0^{-2}$, and ω_0^{-2}, respectively. b is in units of ω_0^{-2}, while λ is dimensionless.)

occurs for low dispersion in the interferometer, long nonlinear crystals, and large mismatch at ω_0 between signal and idler inverse group velocities in the crystal (large Λ).

VIII. CONCLUSIONS

In this paper, we have examined the effect of dispersion on the mutual information that interferometric photon-detection measurements carry about phase shifts. We have looked at a number of different situations involving two interferometer setups and several different types of nonclassical input states. Comparing the results, we now have a precise and quantitative means to measure the relative merits of different input states for various input-parameter ranges. As a by-product, we have shown that in some circumstances, parametric downconversion can be approximated by a much simpler model that is amenable to exact analytical analysis.

Returning to the original question of which input state yields the most information about the phase shift, the graphs of the previous sections yield fairly clear results. Restricting discussion to MZ interferometers for simplicity, we can see that for quantum interferometry in the presence of dispersion the entangled photon pair produced by down-conversion has a clear advantage over other cases when input to a single port (Fock state input). This advantage does not exist in the case of an dispersionless interferometer, in which case the presence or absence of frequency correlations becomes irrelevant for the information content. The only situation we have found in which another input is superior to the frequency-anticorrelated Fock input is when α is large but β small, in which case the anticorrelated *dual* Fock input is superior. These conclusions all hold when the simplified down-conversion model of Sec. IV B is a good approximation; the results of Sec VII imply that such conclusions weaken as the crystal becomes shorter.

ACKNOWLEDGMENTS

This work was supported by a U.S. Army Research Office (ARO) Multidisciplinary University Research Initiative (MURI) Grant, by the Bernard M. Gordon Center for Subsurface Sensing and Imaging Systems (CenSSIS), an NSF Engineering Research Center, and by the Intelligence Advanced Research Projects Activity (IARPA) and ARO through Grant No. W911NF-07-1-0629.

[1] B. Yurke, Phys. Rev. Lett. **56**, 1515 (1986).
[2] B. Yurke, S. L. McCall, and J. R. Klauder, Phys. Rev. A **33**, 4033 (1986).
[3] M. J. Holland and K. Burnett, Phys. Rev. Lett. **71**, 1355 (1993).
[4] J. J. Bollinger, W. M. Itano, D. J. Wineland, and D. J. Heinzen, Phys. Rev. A **54**, R4649 (1996).
[5] E. Knill, R. Laflamme, and G. J. Milburn, Nature (London) **409**, 46 (2001).
[6] H. Lee, P. Kok, N. J. Cerf, and J. P. Dowling, Phys. Rev. A **65**, 030101(R) (2002).
[7] P. Walther, J. W. Pan, M. Aspelmeyer, R. Ursin, S. Gasparoni, and A. Zeilinger, Nature (London) **429**, 158 (2004).
[8] M. W. Mitchell, J. S. Lundeen, and A. M. Steinberg, Nature (London) **429**, 161 (2004).
[9] T. B. Bahder and P. A. Lopata, Phys. Rev. A **74**, 051801(R) (2006).
[10] A. Luis, Phys. Lett. A **329**, 8 (2004).
[11] J. Beltrán and A. Luis, Phys. Rev. A **72**, 045801 (2005).
[12] S. Boixo, A. Datta, M. J. Davis, S. T. Flammia, A. Shaji, and C. M. Caves, Phys. Rev. Lett. **101**, 040403 (2008).
[13] C. K. Hong, Z. Y. Ou, and L. Mandel, Phys. Rev. Lett. **59**, 2044 (1987).
[14] Z. Y. Ou, *Multi-Photon Quantum Interference* (Springer, New York, 2007).